



Synaptic transmission and short-term plasticity at the calyx of Held synapse revealed by multielectrode array recordings

Martin D. Haustein^{a,1}, Thomas Reinert^a, Annika Warnatsch^a, Bernhard Englitz^a, Beatrice Dietz^a, Andrea Robitzki^b, Rudolf Rübsamen^{a,*}, Ivan Milenkovic^a

^a Faculty of Biosciences, Pharmacy and Psychology, University of Leipzig, Leipzig, Germany

^b Center for Biotechnology and Biomedicine (BBZ), University of Leipzig, Leipzig, Germany

ARTICLE INFO

Article history:

Received 28 April 2008

Received in revised form 8 July 2008

Accepted 15 July 2008

Keywords:

Extracellular recordings

Auditory pathways

Mongolian gerbil (*Meriones unguiculatus*)

Medial nucleus of the trapezoid body (MNTB)

Acute brainstem slices

ABSTRACT

We assessed the potential of using multielectrode arrays (MEAs) to investigate several physiological properties of the calyx of Held synapse in the medial nucleus of the trapezoid body of gerbil. Due to the large size of the synapse, it became widely employed in studies on synaptic mechanisms. Electrical stimulation at the midline evoked a characteristic compound signal consisting of a presynaptic volley (C_1) and a postsynaptic response (C_2). The C_1 was blocked by tetrodotoxin, whilst the C_2 was blocked by perfusion of low Ca^{2+} external solution, or the AMPA-R antagonists CNQX, and GYKI52466. NMDA-R blocker D-AP5, partially inhibited the postsynaptic response at P12, but showed no effect in P30 animals. The inhibitory effects of GABA or glycine on postsynaptic responses were reciprocal with regard to animal's maturity: GABA caused a pronounced reduction of C_2 amplitude in P20–22 animals, while glycine showed a stronger inhibition in P27–28 animals. Low-frequency super-threshold stimulation of the afferents induced facilitation of the postsynaptic C_2 amplitudes and only minor changes in temporal characteristics of the signals. At stimulation frequencies >200 Hz, however, significant depression occurs accompanied by increases in transmission delay and in the width of the postsynaptic response. This study suggests MEAs as a useful tool to study calyx of Held synapse by simultaneous recordings of pre- and postsynaptic elements of synaptically interconnected neurons in the auditory brainstem. Moreover, MEAs enable convenient analysis of activity-dependent depression and modulation of neuronal activity by glycine and GABA at later developmental stages not accessible to patch recordings.

© 2008 Elsevier B.V. All rights reserved.

1. Introduction

Simultaneous recording of presynaptic and postsynaptic elements is a prerequisite to understand the properties of synaptic transmission. With this demand, the calyx of Held synapse at the principal cells of the medial nucleus of the trapezoid body (MNTB) became established as a suitable *in vitro* model to investigate excitatory synaptic mechanisms (Forsythe, 1994; Borst et al., 1995). Globular bushy cells of the cochlear nucleus project to the contralateral MNTB and form large, calyx-like terminals, each clasping a single principal neuron (Harrison and Irving, 1966; Friauf and Ostwald, 1988; Spirou et al., 1990; Kuwabara et al., 1991; Smith et al.,

1991). Glutamate release by the calyx of Held terminal mediates reliable transmission with minimal latency fluctuations and well preserved timing of postsynaptic APs during high frequency firing (Banks and Smith, 1992; Oertel, 1999; Trussell, 1999).

Employing extracellular *in vivo* recordings, presynaptic calyceal potentials (“prepotentials”) and postsynaptic action potentials were simultaneously monitored with a single electrode from the MNTB of cats and gerbils (Guinan and Li, 1990; Kopp-Scheinflug et al., 2003a,b). While these experiments have the advantage of acquiring data from an intact neural circuitry, such approach is considerably constrained regarding the application of drugs to scrutinize the details of synaptic transmission. This is possible by simultaneous patch-clamp recordings at the calyx of Held and the principal neuron in *in vitro* preparations, offering an excellent control over the cytoplasm compositions of both neuronal elements and providing a precise picture of synaptical properties at the single cell level. However, paired patch-clamp constellation is difficult to obtain in slices older than 2 weeks and this approach gives only a limited insight into the integration of presynaptic activity during synaptic transmission, which is beneficial in any attempt

* Corresponding author at: Faculty of Biosciences, Pharmacy and Psychology, Institute of Biology II, University of Leipzig, Talstr. 33, D-04103 Leipzig, Germany. Tel.: +49 3419736723; fax: +49 3419736848.

E-mail address: rueb@uni-leipzig.de (R. Rübsamen).

¹ Present address: Department of Cell Physiology and Pharmacology, University of Leicester, Leicester, UK.

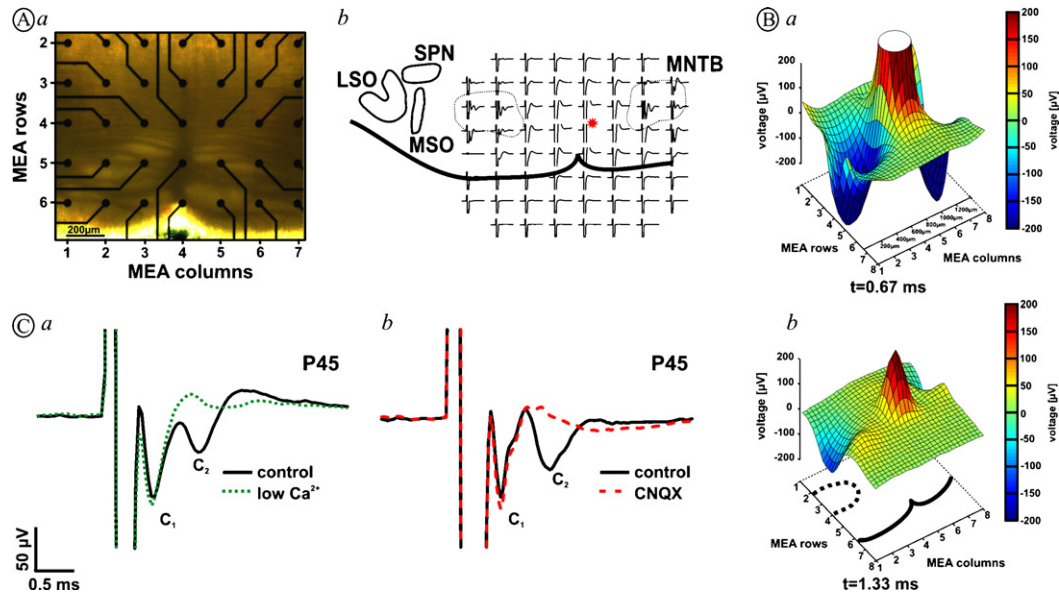


Fig. 1. Multielectrode array (MEA) recordings from acute brainstem slices: (Aa) shows a brainstem slice positioned on a planar MEA. MEA chips had a 8×8 electrode matrix, the actual image shows a section of the chip; inter-electrode distance $200 \mu\text{m}$. (Ab) Schematic representation of a brainstem slice and the signals recorded at the respective positions by the different MEA electrodes upon stimulation close to midline (red asterisk); inter-electrode distance $200 \mu\text{m}$. Characteristic compound signals were recorded in both medial nuclei of the trapezoid body (MNTBs are marked by a dashed line). Nuclei of the superior olivary complex (LSO: lateral superior olive, MSO: medial superior olive, SPN: superior paraolivary nucleus) are shown for better orientation. (B) Electrical maps of evoked activity (constructed from responses to stimulation at the midline, $t=0$) represented at two different time points 0.67 ms (Ba) and 1.33 ms (Bb). Two 3D maps are shown to visualize the propagation of the signals by representing the MEA array as an x, y matrix. The respective signal amplitudes were plotted on the z -axis and pseudocolored. (Ba) Large, positive peak in the middle shows the stimulus artifact and the two negative peaks captured laterally indicate the presynaptic discharge activity. The stimulus artifact was cut off at $200 \mu\text{V}$. (Bb) 1.33 ms after the stimulus, the negative peaks are confined to both MNTB areas (the left one is marked by a dashed line at the basis of the graph, where the thick line indicates the ventral border of the slice). (C) Representative recordings of signals evoked in the MNTB from a P45 gerbil, before (solid lines) and after the application of low- Ca^{2+} ACSF (left panel, dotted line) or CNQX ($50 \mu\text{M}$) (right panel, dashed line). Each trace was the average of 12 runs, 3 pulses each. The two components of the compound signal were termed C_1 and C_2 according to (Guinan and Li, 1990). Impairment of neurotransmission by low- Ca^{2+} ACSF or CNQX blocked the C_2 component while the C_1 component increased slightly in amplitude. Stimulus artifacts were cut off.

to understand neuronal circuitries. The respective experimental conditions give reason for development of a new experimental approach which will bridge the gap between conventional *in vitro* methods and complex but somewhat limited *in vivo* methods. We established a method for extracellular recordings on acute slices of the auditory brainstem by means of multielectrode arrays (MEAs) and investigated properties of synaptic transmission and short-term plasticity in the MNTB. MEAs have become a useful tool to investigate temporal properties of spiking networks, long-term synaptic plasticity, and spatial organization of brain circuit computation in acute brain slices (Novak and Wheeler, 1988; Oka et al., 1999; Egert et al., 2002a; Wirth and Luscher, 2004; Kopanitsa et al., 2006; Mapelli and D'Angelo, 2007). In the present study we show that MEA recordings enable simultaneous investigation of presynaptic and postsynaptic activity in considerably older acute brainstem slices than mostly used for *in vitro* studies (we have used up to P45). We found that the postsynaptic response (mediated by AMPA receptors) was more potentially inhibited by GABA than by glycine at P21–22, whereas glycine exhibited stronger inhibitory effect in older animals (P27–30). Synaptic activity $>200 \text{ Hz}$ induced significant depression of the postsynaptic response and an increase in transmission delay, indicating activity dependent changes in synaptic strength and in the temporal fidelity of neurotransmission.

2. Materials and methods

2.1. Animals and animal care

This study was performed in the Neurobiology Laboratories of the Institute of Biology II at University of Leipzig. All experimental

procedures were approved by the Saxonian district Government, Leipzig, and they were done according to European Communities Council Directive of 24 November 1896 (86/609/EEC).

2.2. Slice preparation and maintenance

Acute brainstem slices ($300 \mu\text{m}$) containing the MNTB were cut by means of vibratome (Microm HM 650, Walldorf, Germany) as previously described (Forsythe, 1994) from Mongolian gerbils (*Meriones unguiculatus*) aged postnatal day twelve to forty-five (P12–45). Briefly, transverse slices were cut in the cold ($3\text{--}4^\circ\text{C}$) low-calcium, low-sodium solution containing (in mM): 2.5 KCl , 0.1 CaCl_2 , 4 MgCl_2 , $1.25 \text{ NaH}_2\text{PO}_4$, 25 NaHCO_3 , 10 glucose , 250 sucrose , $2 \text{ sodium pyruvate}$, 3 myo-inositol , $0.5 \text{ ascorbic acid}$, continuously equilibrated with $5\% \text{ CO}_2$ and $95\% \text{ O}_2$, pH 7.4. The slices were preincubated for 30 min at 37°C and stored at room temperature (RT), for at least 30 min , until recording in extracellular solution (ACSF) of the following composition (in mM): 125 NaCl , 2.5 KCl , 2 CaCl_2 , 1 MgCl_2 , $1.25 \text{ NaH}_2\text{PO}_4$, 25 NaHCO_3 , 10 glucose , $2 \text{ sodium pyruvate}$, 3 myo-inositol , $0.5 \text{ ascorbic acid}$, pH 7.4 when equilibrated with $5\% \text{ CO}_2$ and $95\% \text{ O}_2$ mixture. In experiments in which transmitter release was blocked, Ca^{2+} was reduced to 0.1 mM and Mg^{2+} increased to 2.9 mM .

Tight contact between MEA electrodes and the slice was achieved by coating MEAs with nitrocellulose solution ($4 \mu\text{l}$; 0.14 mg/ml dissolved in methanol) and leaving them to air dry (Egert et al., 2002a). Whole brainstem slices were positioned with both MNTB areas over the electrode field (see Fig. 1) and remaining ACSF between the slice and MEA was removed using filter paper. Slices were superfused with gassed ACSF at the rate of 0.8 ml/min through the recording chamber (volume 1.5 ml). Recordings were

done on the stage of an inverse microscope (Axiovert 200, Zeiss, Germany), at RT, unless otherwise noted.

2.3. MEA recordings and data analysis

We used arrays of 60 planar titanium nitride-coated electrodes (Multi Channel Systems (MCS), Reutlingen, Germany). Each electrode was 30 μm diameter with 200 μm separation between electrodes and arranged in a 8×8 grid. Signals were measured against a bath electrode and amplified 1200 \times at a sampling rate of 25 kHz, using a 60-channel MEA-amplifier (MEA-1060, MCS). FP were negative with respect to ground electrode and thus shown as negative deflections from the baseline. According to electrophysiological conventions, the sink (inward positive) currents indicate membrane excitation. Calyceal axons originating from globular bushy cells in the CN were stimulated at the midline where they cross to the contralateral side and innervate principal cells of the MNTB (Kuwabara et al., 1991). Evoked FP represent the summed potentials in a population of neurons and were typically recorded from 2 to 3 electrodes lying directly underneath the visually identified MNTB. The principal cells are by far the dominant cell type in the MNTB (Casey and Feldman, 1982); they are characterized by large somata giving rise to one or two primary slender dendrites (Morest, 1968; Sommer et al., 1993). Single unit neuronal activity can be detected with MEA electrodes within a range of up to 100 μm from the respective neurons (Egert et al., 2002a). Concordantly, adjacent electrodes are not likely to record potentials from the same neuron when the electrode spacing is 200 μm (Lin et al., 2005). However, given the recordings of evoked local FP in our study, some overlap between the information represented in the signals from flanking electrodes would be conceivable.

Commercially available software, MC Rack and MC Stimulus (MCS) were employed for data acquisition, analysis and stimulation. Electric stimuli were generated by a STG 1004 stimulus generator (MCS); biphasic pulses ($\pm 10 \mu\text{A}$ to $\pm 90 \mu\text{A}$, 80 μs /phase) were applied via a monopolar tungsten electrode (diameter 125 μm ; Science Products, Hofheim, Germany). In each slice, the electrode position, approximately 500 μm from recording electrodes, was photographed to reconstruct the stimulation site. After positioning the stimulation electrode at the midline, super-threshold stimulation consisting of 3 pulses at 50 Hz was applied every 5 s (test pulse) for 5 min before the experiment was started. This was done to control for quality of recording and to minimize the effects of synaptic depression at the calyx of Held synapse which was recently shown to be more pronounced at the onset of stimulation in acute brainstem slices that were silent prior to experiment (Hermann et al., 2007). The same test pulse protocol (3 pulses at 50 Hz, every 5 s) was thereafter constantly applied during each experiment to obtain the same recording conditions in all slices, unless the experimental design required alterations of the stimulation protocol.

Data analysis was performed off-line using MEA-Tools (Egert et al., 2002b) for Matlab Version 6.1 (The Mathworks Inc., MA, USA), and custom designed routines also written in the Matlab. The amplitudes of the neuronal discharges were determined by measuring negative peaks in a defined time window as previously recommended by Johnston and Wu (1995). Briefly, the (negative) peak amplitude is determined by an automatic Matlab-procedure measuring the distance between the minimum of the negative peak and a point that corresponds to the projection of this minimum to the line joining the two flanking positive peaks (peak-base) (see Inset in Fig. 3B). The width of the signal components was measured as the time at 50% of the respective peak amplitude. Unless otherwise noted, the results were quantified as mean \pm S.E.M. Groups of data were compared by Student's *t*-test or one-way ANOVA.

To determine the effects of drugs on the relative FP amplitude (Figs. 2B and 4), the data were compared to those of control recordings, also performed with 3 pulses at 50 Hz, applied in 5 s intervals.

3. Results

3.1. Evoked field potentials recorded from the MNTB

Electrical stimulation at the midline was used to stimulate afferents of the principal MNTB neurons (Forsythe and Barnes-Davies, 1993b). Super-threshold stimuli gave complex, multi-unit field potentials within the MNTB, in 74 slices obtained from P12 to P45 gerbils. Such field potentials typically consisted of two distinct components (Fig. 1Ab and C), similar to the compound signals previously observed after electrical stimulation and recording of single units *in vivo*, termed C_1 and C_2 (Guinan and Li, 1990). In our study, both signal components were negative voltage deflections indicating successive membrane depolarizations with their amplitudes depending on the stimulus intensity.

We first explored the biological nature of these compound waveforms. To distinguish between presynaptic and postsynaptic signal components we impaired the transmitter release by perfusing low- Ca^{2+} , high- Mg^{2+} ACSF (Borst et al., 1995). This caused a reduction of the C_2 component by $-89 \pm 3\%$ ($n=23$ electrodes, 9 slices, $p < 0.001$) (Fig. 1Ca). At the same time, the C_1 component was transiently increased by $14 \pm 2\%$ ($p < 0.001$), and positive voltage deflection became visible following the negative peak of C_1 . Similar observations were made in patch-clamp studies at the calyx of Held, where the presynaptic APs showed a pronounced after-hyperpolarization followed by a small depolarizing after-potential (Borst et al., 1995; Taschenberger and von Gersdorff, 2000; Dodson et al., 2003). The latter signal component probably reflects the discharge of the internodal membrane capacitance of the large axon (Barrett and Barrett, 1982). The C_2 component indicates the summed excitatory postsynaptic response, since it was blocked by AMPA/kainate receptors antagonist, such as CNQX (25 μM , Tocris). The CNQX application reduced the C_2 amplitude by $-104 \pm 4\%$, while at the same time it increased the C_1 component by $21 \pm 3\%$ ($n=26$ electrodes, 9 slices, for both components $p < 0.001$) (Fig. 1Cb). The reduction of the C_2 component by more than 100% is due to a positive shoulder at the tail-end of the C_1 component, which becomes visible when the C_2 is blocked, and which affects the base line providing the reference values for amplitude measurements (see also Fig. 1Ca). In previous experiments it was shown that in MNTB principal cells of young rats (P6–16) the stimulation of afferents evokes dual-component EPSCs which were mediated both by NMDA and AMPA receptors (Forsythe and Barnes-Davies, 1993a). Therefore, we measured the C_2 components while stimulating with a 5-pulse-train at 100 Hz and compared the responses in the absence or in the presence of D-AP 5 (100 μM , Tocris), a specific blocker of NMDA receptors (Fig. 2). In P12 animals, the 5th C_2 components revealed (i) a D-AP 5-induced reduction by $-39 \pm 6\%$ compared to the respective control condition, (ii) an increase in C_1 -to- C_2 delay by $250 \pm 3 \mu\text{s}$, and (iii) an enlargement of the half-width of C_2 by $214 \pm 8 \mu\text{s}$ ($n=3$ electrodes, 2 slices, $p < 0.001$) (Fig. 2A Inset). In P30 gerbils, we did not observe NMDA receptor components in C_2 ($n=6$ electrodes, 2 slices; Fig. 2A). However, in slices of the same postnatal age the application of AMPA receptor antagonist GYKI 52466 (100 μM , Tocris) efficiently blocked the C_2 amplitude by $-93 \pm 2\%$ ($n=6$ electrodes, 2 slices, $p < 0.001$), consistent with AMPA receptor-mediated signaling (Fig. 2Ab). The opposite effect, namely an increase by $25 \pm 1\%$ ($p < 0.001$) was observed for the C_1 component in the same slices. This was similar to the effect of CNQX (Fig. 1Cb).

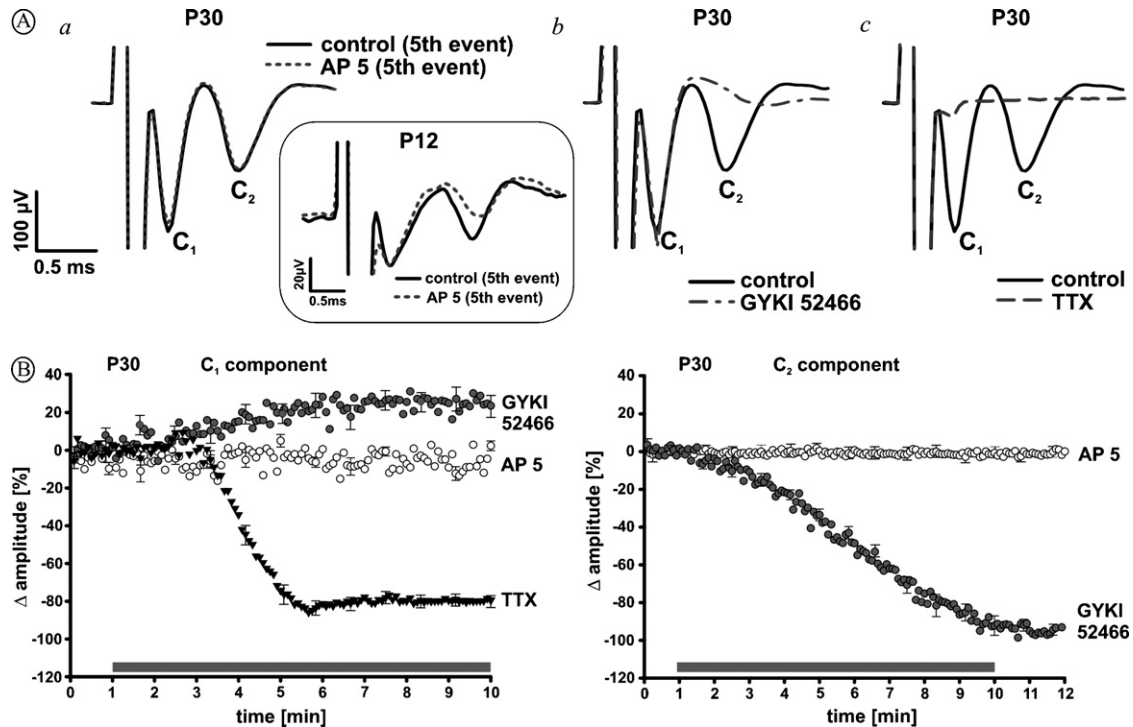


Fig. 2. Characterization of pre- and postsynaptic components of evoked field potentials. (A) Representative recordings from the MEA electrodes located under the MNTB showing the effects of D-AP 5, GYKI 52466, and TTX on the evoked field potentials. The electrical traces are averages of 12 runs, 3 pulses each. Stimulus artifacts were cut off for clarity. (Aa) In P30 animals, NMDA receptor antagonist D-AP 5 (100 μ M) had no effect on recorded signals at 100 Hz synaptic stimulation. Inset, FP recorded from P12 gerbil, generated by a 100 Hz train. Under D-AP 5 (grey dashed line), the C_2 amplitude is reduced, while synaptic latency and signal width are increased compared to the control (black solid line). (Ab) Application of AMPA receptor antagonist GYKI 52466 (100 μ M) abolished the C_2 component, whereas the C_1 amplitude was slightly increased. (Ac) The C_1 component was almost completely abolished by the Na^+ channel blocker TTX (500 nM). (B) Mean time course of the relative changes in C_1 (left panel) and C_2 (right panel) amplitudes during application of D-AP 5 (100 μ M), GYKI 52466 (100 μ M), and TTX (500 nM) in 30-day-old gerbils. While D-AP 5 had no effect on recorded signals ($n=6$ electrodes, 2 slices P30), GYKI 52466 increased the C_1 amplitude by $25 \pm 1\%$ ($p < 0.001$, ANOVA) and reduced C_2 by $-93 \pm 2\%$ ($n=6$ electrodes, 2 slices P30, $p < 0.001$, ANOVA). Under TTX, the amplitudes of C_1 were maximally reduced by $-89 \pm 5\%$ ($n=6$ electrodes, 2 slices P30, $p < 0.001$, ANOVA). Bars indicate application time. Error bars indicate \pm S.E.M.

To clarify the nature of the C_1 component, the slices were (after undergoing the blockade with GYKI 52466) perfused with tetrodotoxin (TTX, 500 nM, Tocris) to block the afferent AP propagation. The addition of TTX almost completely blocked the C_1 component ($-89 \pm 5\%$; $n=6$ electrodes, 2 slices, $p < 0.001$), indicating its presynaptic origin (presynaptic volley) (Fig. 2Ac and B, left).

3.2. Characteristics of field potentials as a function of stimulus intensity and stimulation frequency

In patch clamp recordings, afferent fiber stimulation evoked short latency all-or-nothing prespikes which were rapidly followed by large EPSCs (Forsythe, 1994). Current clamp recordings revealed that MNTB principal neurons respond to a steady depolarization with a characteristic single AP, even with depolarizations well exceeding the threshold (Forsythe and Barnes-Davies, 1993b). We next explored the stimulus-response relation in FP recorded with MEA. First we determined the stimulus intensity which evoked FP with C_2 amplitudes exceeding at least twice the standard deviation of the noise. In 16 of 17 electrodes analyzed (7 slices) this criterion was met with biphasic 15 μ A stimuli evoking mean C_1 amplitudes of $-22 \pm 2 \mu$ V and C_2 amplitudes of $-9 \pm 1 \mu$ V (Fig. 3A). Raising the stimulus intensity to 20 μ A resulted in significant responses at all 17 electrodes considered ($C_1 = -53 \pm 5 \mu$ V, $C_2 = -18 \pm 2 \mu$ V, $p < 0.05$). Stimulus-response curves for C_1 and C_2 showed a steady increase up to 40 μ A, and for higher stimulus intensities a rectification, indicating that the maximal response amplitudes for the pre- and the postsynaptic components are approached (for

stimuli of 30 μ A $C_1 = -100 \pm 7 \mu$ V, $C_2 = -42 \pm 2 \mu$ V; for 40 μ A $C_1 = -118 \pm 8 \mu$ V; $C_2 = -62 \pm 5 \mu$ V; for 50 μ A $C_1 = -124 \pm 9 \mu$ V; $C_2 = -71 \pm 6 \mu$ V; for 60 μ A $C_1 = -124 \pm 10 \mu$ V; $C_2 = -76 \pm 6 \mu$ V; for 90 μ A $C_1 = -130 \pm 13 \mu$ V; $C_2 = -82 \pm 7 \mu$ V; $n=17$ electrodes, 7 slices) (Fig. 3A). Up to 40 μ A, stimulation at the midline apparently activated successively more fibers terminating in calyx synapses in the catchment area of single electrodes of the MEA and, consequently, triggered firing in more postsynaptic neurons. Towards higher stimulus amplitudes, pre- and postsynaptic response amplitudes levelled off indicating complete recruitment of the afferents and postsynaptic MNTB neurons recorded by a single MEA electrode. Under these conditions the C_1 and the C_2 components presumably represent the summed activity of respective pre- and postsynaptic spikes. For the study of the effect of drugs on pre- and postsynaptic discharge activity, stimulus intensity inducing half-maximal C_2 response was determined and used throughout. Typical value was 30 μ A, which caused an average ratio of C_1/C_2 amplitudes of 2.4 ± 0.2 .

At room temperature, the average peak delays for C_1 and C_2 , measured from the peak of the stimulus artifact, were 0.67 ± 0.02 ms and 1.33 ± 0.03 ms, respectively ($n=1152$ stimulations, 24 electrodes from 13 slices), which yields a C_1 -to- C_2 delay of 0.66 ± 0.02 ms. At physiological temperature (35 $^{\circ}$ C), C_1 -to- C_2 delay was 0.45 ± 0.01 ms and the average peak delays for C_1 and C_2 were considerably shorter (0.60 ± 0.02 ms and 1.05 ± 0.01 ms, respectively). We termed the time from the peak of the stimulus artifact to the peak of the C_2 component *transmission delay* (Fedchyshyn and Wang, 2007), which is defined by the sum of (i) the *conduction delay* (time from the peak of the stimulus artifact to the peak of the presy-

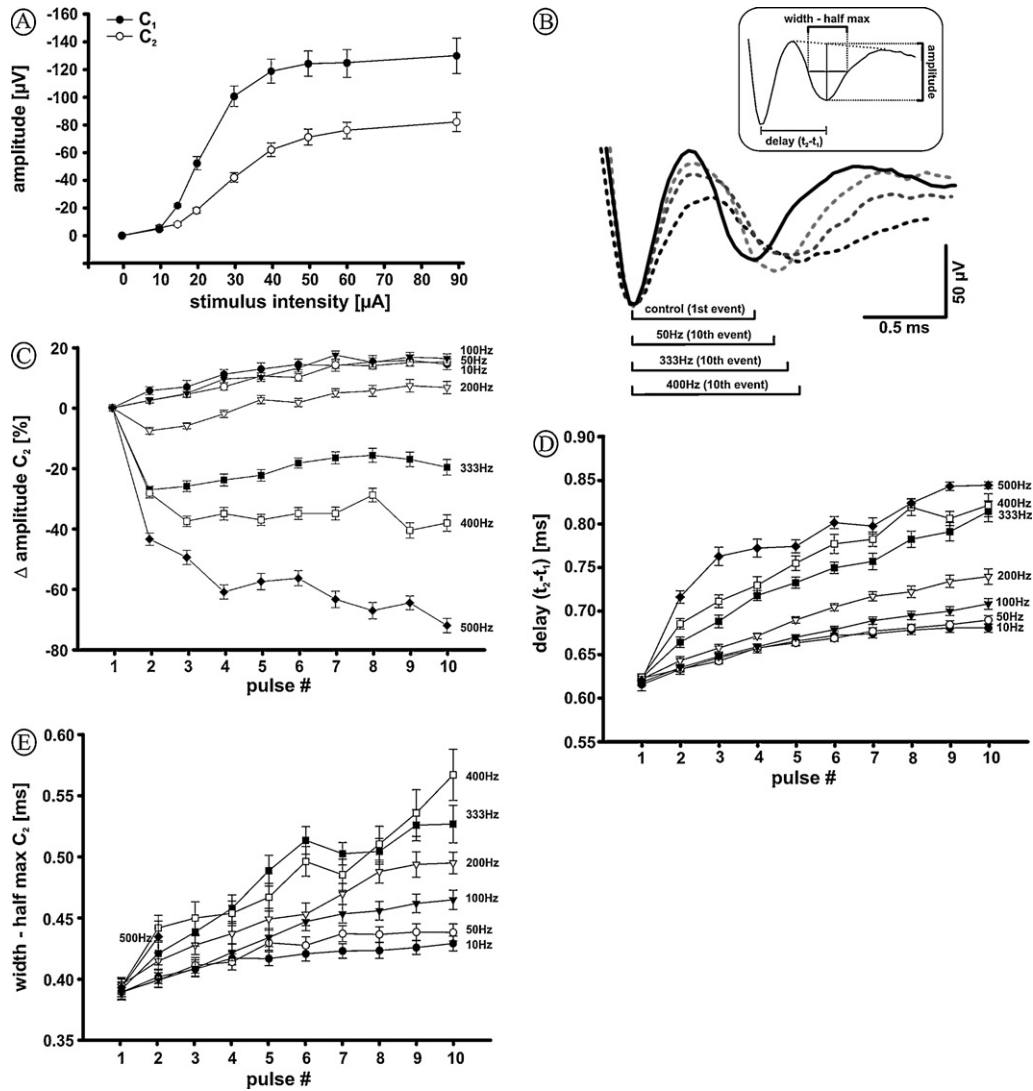


Fig. 3. Activity-dependent changes in amplitude and timing precision of evoked field potentials measured in P30–45 slices. (A) Amplitudes of FP components (C_1 and C_2) were measured at their peak and shown as a function of stimulus intensity. The response threshold for the presynaptic (C_1) and the postsynaptic (C_2) response was reached at the current stimulation of $15 \mu\text{A}$; a stimulus-dependent increase in response amplitude was seen up to the stimulus intensities of $40 \mu\text{A}$ (C_1) and $50 \mu\text{A}$ (C_2). Towards higher stimulus intensities both responses components show rectification ($n = 22$ electrodes, 9 slices). (B) Averaged FP (10 runs, 10 pulses each) evoked at different stimulation frequencies. To facilitate comparison of the waveforms, traces were aligned at the negative peak of C_1 , as previously done to analyse the data from patch recordings (Taschenberger and von Gersdorff, 2000). Black solid line shows the compound field potential to the first of 10 successively presented stimuli which are highly constant at the different stimulus conditions. The different grey dashed lines show the 10th response of a stimulus series presented at the frequencies indicated below the graphs. Note that with increasing stimulus frequencies the C_2 amplitude decreases and the latency and signal width increase. Inset, Description of parameters used to analyse signal properties. (C) Frequency-dependent changes of the postsynaptic responses during a 10-pulse-train. Relative changes in postsynaptic amplitude (C_2) show slight facilitation for stimulation frequencies up to 100 Hz. At 200 Hz, transient depression of early events was observed. Input frequencies >200 Hz induce depression which either can reach a steady state (after the 2nd or the 3rd event for 333 and 400 Hz, respectively), or continues to increase during 500 Hz trains ($n = 10$ electrodes, 6 slices). (D) Prolongation of C_1 – C_2 delay to successive stimuli in a 10-pulse-series and for different stimulus repetition rates. Note that an ongoing increase in latency was observed for all stimulus repetition rates, and that this effect was augmented towards higher repetition rates ($n = 10$ electrodes, 6 slices). (E) Half-width of the postsynaptic response indicates progressive broadening of the signals with increasing stimulation frequency ($n = 10$ electrodes, 6 slices). During the 500 Hz stimulation only first two responses could be measured, since the repolarizing phases of C_2 more and more overlapped with the subsequent stimulus artifacts.

naptic component), (ii) the *synaptic delay* (time from the peak of the presynaptic component to the onset of the postsynaptic response), and (iii) the *response rise delay* (the time interval between the onset and the peak of the postsynaptic response, which provides a measure of synchronicity of release events). Systematic analysis of the respective data yielded that, in a train of three pulses applied at 50 Hz, the conduction delay remained unchanged (0.67 ± 0.02 ms) while the transmission delay increased from 1.33 ± 0.03 ms for the first pulse to 1.36 ± 0.03 ms for the second and to 1.38 ± 0.03 ms for the third pulse ($p < 0.001$, $n = 1152$ stimulations, 24 electrodes from 13 slices). This data indicated that already a 50 Hz-stimulation

induces in successive neuronal discharges an increase in synaptic- and/or response rise delay, indicating a tendency for desynchronization of postsynaptically evoked responses.

To further address this issue, we investigated evoked FP at various stimulation frequencies. For this purpose, trains of 10 pulses were applied at the rate of 10, 50, 100, 200, 333, 400, and 500 Hz, and the amplitudes and the temporal characteristics of C_1 and C_2 components of the signals were compared (Fig. 3B–E). Inspection of the data in Fig. 3B and C revealed differences in postsynaptic responses with regard to stimulation frequency: (i) a facilitation of C_2 amplitudes was observed in response to test trains between 10

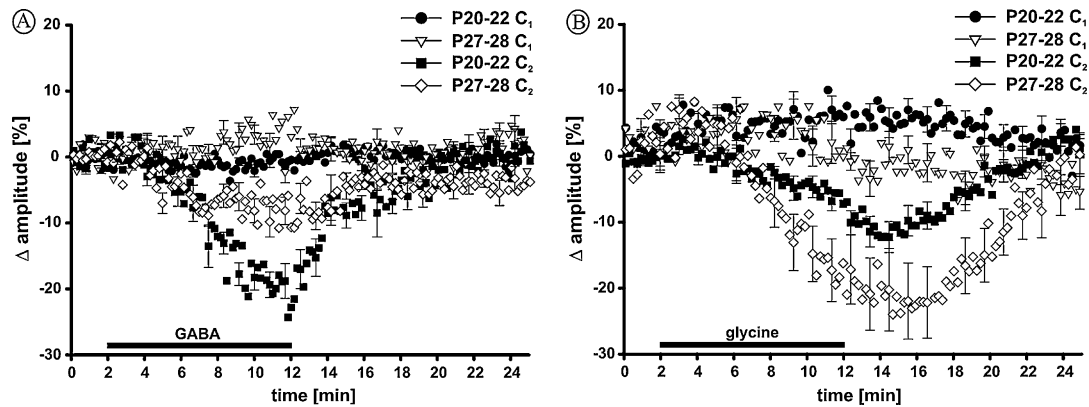


Fig. 4. Effects of GABA and glycine on the relative amplitudes of evoked FP. (A) Application of GABA reduced the amplitude of the postsynaptic component (C_2) by maximally $-20.6 \pm 0.6\%$ in P20-22 ($n = 18$ electrodes, 6 slices, $p < 0.001$, ANOVA) and by $-7.9 \pm 6.5\%$ in P27-28 ($n = 23$ electrodes, 5 slices, $p < 0.001$, ANOVA) animals. The inhibitory effects were significant in both age groups, yet significantly different when the two groups were compared ($p < 0.001$, ANOVA). Perfusion of GABA evoked no significant changes of the presynaptic component (C_1) in both age groups ($-0.7 \pm 0.2\%$ in P20-22 and $3.1 \pm 0.7\%$ in P27-28 group, $p = 0.52$, ANOVA). (B) Significantly stronger inhibition of the postsynaptic (C_2) component was observed in older animals after application of glycine (reduction by $-11.5 \pm 2.3\%$ and by $-20.1 \pm 5.9\%$ in P20-22 and P27-28, respectively; P20-22 $n = 26$ electrodes, 6 slices; P27-28 $n = 25$ electrodes, 6 slices, $p < 0.001$, ANOVA). With a similar time-course, glycine evoked a significant increase of the presynaptic (C_1) component in both age groups ($6.1 \pm 0.3\%$ in P20-22; $7.5 \pm 0.3\%$ in P27-28; ($p < 0.05$, ANOVA)). The effects of glycine on C_1 were not significantly different between the two developmental stages tested. Application bars indicate duration of perfusion.

and 100 Hz, possibly reflecting an action of residual Ca^{2+} on glutamate release (Sakaba and Neher, 2001b), (ii) at 200 Hz, a slight transient depression (2nd response decreased by $-8 \pm 1\%$, 3rd by $-6 \pm 1\%$) was followed by scarcely increased amplitudes of later responses (10th response increased by $7 \pm 2\%$), (iii) a prominent depression of the C_2 component was observed when the stimulation frequency was further increased: decrease in the 2nd response by $-27 \pm 1\%$ at 333 Hz, by $-28 \pm 2\%$ at 400 Hz, and by $-44 \pm 2\%$ at 500 Hz ($n = 7$ electrodes, 4 slices). The C_2 amplitudes reached a more or less steady-state after the 2nd response at 333 Hz stimulation, after the 3rd response at 400 Hz (reduction by $-38 \pm 2\%$), while the amplitudes evoked at 500 Hz showed an exponential decay with each subsequent pulse in the train (amplitude of 10th signal was reduced by $-72 \pm 2\%$). In addition to the frequency-dependent depression in C_2 , we assessed changes of the C_1 – C_2 peak delay, which indicates the sum of synaptic delay plus response rise delay of the C_2 component (Fig. 3D). As for the changes in C_2 amplitude, there were only slight changes in the C_1 – C_2 delay up to 200 Hz stimulus frequencies. Yet, for higher frequencies up to 500 Hz (the highest frequency tested) the prolongation of the C_1 – C_2 delay was more pronounced throughout the series of evoked discharges (Fig. 3D). The average increase in latency between 1st and 10th response was $64.9 \pm 4.8 \mu\text{s}$ for 10 Hz, $66.8 \pm 5.1 \mu\text{s}$ for 50 Hz, $90.2 \pm 6.2 \mu\text{s}$ for 100 Hz, $117.8 \pm 8.9 \mu\text{s}$ for 200 Hz, $191.1 \pm 12.0 \mu\text{s}$ for 333 Hz, $197.7 \pm 13.1 \mu\text{s}$ for 400 Hz, and $224.0 \pm 4.8 \mu\text{s}$ for 500 Hz ($n = 7$ electrodes, 4 slices). We next asked whether the response rise delay which provides a measure of the synchronicity of release events might contribute to the activity-dependent prolongation in transmission. Since an accurate measurement of the onset of C_2 is difficult to achieve (for an evaluation of analytical approaches to the quantification of temporal delays see Fedchyshyn and Wang, 2007), we measured the half-maximal width of the C_2 , as an indirect estimate of the response rise delay. The half-maximal widths were plotted against the stimulus numbers for different stimulation frequencies (Fig. 3E). The widths of the signals progressively increased towards higher discharge rates, indicating gradual reduction in synchronicity of release events. The respective increase in the width between the 1st and 10th response was $39.8 \pm 6.0 \mu\text{s}$ for 10 Hz, $48.4 \pm 7.0 \mu\text{s}$ for 50 Hz, $75.7 \pm 7.9 \mu\text{s}$ for 100 Hz, $99.4 \pm 8.8 \mu\text{s}$ for 200 Hz, $135.0 \pm 15.4 \mu\text{s}$ for 333 Hz, and $173.1 \pm 20.1 \mu\text{s}$ for 400 Hz. At 500 Hz stimulation, the measurement of the half-maximal response was only possible for the first 2 sig-

nals. In later signals, the repolarizing phase of C_2 progressively overlapped with the stimulus artifacts of the successive stimulus. The changes in the half-maximal width of the postsynaptic response cannot solely account for the prolongation in the C_1 – C_2 peak delay. Thus, these results strongly indicate that at least two temporal components of synaptic transmission (synaptic delay and response rise delay) contribute to the activity-dependent changes in the temporal fidelity at the calyx of Held synapse.

3.3. Effects of GABA and glycine on recorded FP

In addition to the calyceal excitatory input, through which a single afferent fiber effectively drives a principal cell of the MNTB, additional synaptic signalling conveyed by glycine and GABA contributes to the fidelity of this synapse (Banks and Smith, 1992; Wu and Kelly, 1995; Awatramani et al., 2004). MEA recordings offer a possibility to simultaneously monitor the effects of respective inhibitory neurotransmitters on both the presynaptic and the postsynaptic components of the evoked FP. First, we employed the midline stimulation to activate the excitatory inputs through the calyx of Held and investigated the effects of antagonists of GABA_A and glycine receptors, gabazine (SR 95531, 25 μM , Tocris) and strychnine (1 μM , Research Biochemicals International), respectively. Mere inhibition of GABA_A had no influence on MNTB signals in $n = 11$ electrodes, 5 slices. On the other hand, following the application of strychnine in P27–30 slices, the C_1 component was significantly reduced ($-10.5 \pm 1.8\%$) while the C_2 component remained unchanged ($3.4 \pm 0.1\%$) ($n = 8$ electrodes, 4 slices) (data not shown). We further investigated the effects of GABA and glycine, applied by bath perfusion, on FP evoked through the midline stimulation. Due to the opposite effects of the presynaptic GABA_A and GABA_B receptors on release of glutamate (Isaacson, 1998; Kajikawa et al., 2001; Turecek and Trussell, 2002), the latter were blocked by CGP 54626 (10 μM) during perfusion of GABA (1 mM). Application of GABA reduced the amplitude of the C_2 components of the evoked FP, with the magnitude of the effect being dependent on the animal's age. Maximal GABA-induced reduction of the C_2 component was $-20.6 \pm 0.6\%$ in P20-22 ($n = 18$ electrodes, 6 slices, $p < 0.001$) (Fig. 4A). A similar, albeit significantly less pronounced effect was observed in P27-28 gerbils (reduction by $-7.9 \pm 6.5\%$; $n = 23$ electrodes, 5 slices, $p < 0.001$) ($p < 0.001$ for P20-22 vs. P27-28). GABA did not change the C_1 amplitude indicating that the effect is likely

to occur postsynaptically (Fig. 4A). Perfusion of glycine (1 mM) significantly reduced the C_2 component by $-11.5 \pm 2.3\%$ and by $-20.1 \pm 5.9\%$ in P20–22 and P27–28 animals, respectively (P20–22 $n=26$ electrodes, 6 slices, $p < 0.001$; P27–28 $n=25$ electrodes, 6 slices, $p < 0.001$) (Fig. 4B).

In contrast to the influence of GABA, the inhibitory effect of glycine was significantly stronger in older animals (for P20–22 vs. P27–28 $p < 0.001$). Another difference between GABA and glycine was seen in terms of the effect on the C_1 component. Glycine evoked a slight but significant transient increase of the C_1 amplitude by $6.1 \pm 2.2\%$ in P20–22 and by $7.5 \pm 0.3\%$ in P27–28 animals (for P20–22 vs. P27–28 $p = 0.54$) (Fig. 4B). However, this increase in C_1 was not accompanied by an enlargement, but rather by a reduction of the C_2 amplitude, suggesting that higher glycine concentrations might predominantly exert an inhibitory postsynaptic effect. Both the effects of GABA and glycine were reversible; after washout the amplitudes of the evoked FP returned to the control levels (Fig. 4). The inhibitory effects of GABA and glycine were efficiently blocked by gabazine and strychnine, respectively (data not shown). Taken together, these data are congruent with the current view of the inhibitory postsynaptic effects of GABA and glycine in P20–28 MNTB, whereas the depolarization at a presynaptic level is, at this developmental stage, caused by glycine only.

4. Discussion

We assessed the local evoked FP in the MNTB of acute brainstem slices of the gerbil and characterized the recorded signals with specific reference to previous *in vitro* and *in vivo* studies. To our knowledge, this is the first description of MEA recordings obtained from an *in vitro* preparation of the auditory brainstem. Four main findings emerged from the present endeavor: Electrical stimulation of MNTB afferents triggered (1) characteristic compound signals composed of presynaptic (C_1) and postsynaptic components (C_2). (2) Super-threshold stimulation up to 100 Hz induced a slight facilitation of the C_2 amplitudes, yet at stimulation frequencies >200 Hz signal amplitudes gradually decreased and the C_1 – C_2 delay increased along with the width of C_2 . (3) Superfusion of GABA caused a reduction in the amplitude of C_2 , the effect being more pronounced in animals at P20–22 than at P27–28. (4) Glycine induced a transient increase in the amplitude of C_1 (independent of the animals' postnatal age) while it had a stronger inhibitory effect on C_2 in older animals (P27–28).

4.1. Complex waveforms of evoked field potentials in the MNTB

No spontaneous spiking activity was observed in the MNTB. Spontaneous activity is lost in auditory domains of brainstem slices due to deprivation of spontaneously firing auditory nerve fibers (Liberman, 1978; Geisler et al., 1985) which were cut off during preparation. Electrical stimulation in a midline position of the trapezoid body evoked characteristic voltage signals consisting of two distinct components at electrodes underneath the MNTB. No such signals were picked up by electrodes of the MEA chip located outside the borders of the MNTB, indicating that the evoked voltage signals reflect a specific MNTB activity associated with the activation of afferent excitatory fibers.

A number of electrophysiological studies reported separation of pre- and postsynaptic signal components in recordings from MNTB principal cells and from spherical bushy cells of the cochlear nucleus. Signals were assessed either by extracellular single unit recordings *in vivo* (cat: Guinan and Li, 1990; gerbil: Kopp-Scheinflug et al., 2002, 2003a; Green and Sanes, 2005; guinea pig: Winter and Palmer, 1990) or by single electrode intra-

cellular or loose-patch recordings *in vitro* (mouse: Wu and Kelly, 1993; gerbil: Hermann et al., 2007). In these studies the pre- and postsynaptic components were typically separated by 0.4–0.9 ms and these data match well with our values obtained at RT and at physiological temperature. With respect to the data presented here, the presynaptic origin of the C_1 component was confirmed by its obliteration following the perfusion of TTX, same as previously shown in patch recordings (Forsythe, 1994; Borst et al., 1995; Leao et al., 2005). Evidence for classification of C_2 as the postsynaptic component came from blocking synaptic transmission by superfusion of low calcium ACSF or blocking the AMPA receptors with GYKI 52466. Both approaches selectively inhibited the C_2 component. Pharmacological characterization of the signals revealed that C_1 represents integrated volleys of discharges of presynaptic elements, which terminate on MNTB principal cells and synaptically evoke the responses summed up in the C_2 component.

Different sources of C_1 and C_2 components are also evidenced by the responses to changes in the strength of electrical stimulation. The intensity–response curves for both signal components have the same threshold and, for all super-threshold stimulus intensities the C_1 amplitudes are larger than the C_2 amplitudes. For stimulus intensities between 15 and 40 μA , there is an almost linear increase in the signal amplitudes of C_1 and C_2 and the amplitude ratio between both components stayed in a narrow range ($C_1/C_2 = 2.4$ for 15 μA and $C_1/C_2 = 1.9$ for 40 μA stimulation). This is in accordance with the recruitment of neighbouring fibers with increasing stimulus strength leading to an activation of additional principal neurons. At 50 μA and above, both response curves show saturation indicating that C_1 and C_2 originate from (a limited number of) afferent calyceal terminals and principal cells located close to a respective MEA-electrode, all of which produce distinct, precisely timed discharges (C_1/C_2 amplitude ratio 1.6–1.7). The synchronous generation of a brief postsynaptic AP from a population of principal neurons can be explained by prominent outward rectifying potassium conductance ($g_{\text{K}L}$: low threshold and $g_{\text{K}H}$: high threshold) which has been described in auditory neurons, known to receive and convey information in the timing of firing (Trussell, 1999).

Earlier *in vitro* studies reported age-dependent changes in the contribution of different glutamate receptors to the postsynaptic EPSC (Futai et al., 2001; Joshi and Wang, 2002). The accessibility of older animals in MEA recordings prompted us to reevaluate this issue. A contribution of NMDA-receptors to the C_2 component was observed at P12 but not at P30 (Fig. 2). By then, the C_2 component is solely dependent on the AMPA receptor activation, which is consistent with results from previous patch-clamp studies in rat and mice (Taschenberger and von Gersdorff, 2000; Futai et al., 2001; Joshi et al., 2004).

In contrast to the inhibitory effect of AMPA receptor-blockers on the C_2 amplitude, the C_1 amplitude showed a significant increase following the application of CNQX or GYKI 52466.

This effect on the C_1 amplitude is unexpected and it cannot be explained by the current literature data. Presynaptic AMPA receptors at the calyx of Held have been shown to inhibit Ca^{2+} currents by means of G proteins and thereby regulate transmitter release (Takago et al., 2005). Therefore, the inhibition of presynaptic AMPA receptors could possibly potentiate Ca^{2+} currents in our experiments. Still, it is rather unlikely that this modulation of the presynaptic Ca^{2+} current could account for an increase in C_1 amplitude of about 20%. We also assessed the C_1/C_2 amplitude ratios for two different latencies, i.e. RT and 35 °C, to examine whether the C_1 amplitude might be affected by the changes of C_2 due to a partial overlap of the two signals. At 35 °C the C_1 and C_2 amplitudes decreased to about 80% of their initial values at RT, however, the C_1/C_2 ratio did not significantly change with shorter synaptic latency. This implies that the C_1 and C_2 components are largely

independent, thus inhibition of C_2 is unlikely to account for the increase in C_1 amplitude after CNQX and GYKI 52466.

Despite the lack of an interpretation of the effects on C_1 , the respective changes would not interfere with our observation that signal transmission at the subadult calyx of Held principal neuron synapse is solely mediated by AMPA receptors.

4.2. Activity-dependent changes of transmission properties

The calyx of Held synapse is specialized for preserving timing information during synaptic transmission in the brainstem sound localization pathway (Oertel, 1999; Trussell, 1999). This is reflected in the ability to follow high-frequency electrical stimulation and trigger postsynaptic EPSP at the same rate, as shown in numerous *in vivo* and *in vitro* studies (Spirou et al., 1990; Banks and Smith, 1992; Wu and Kelly, 1993; Taschenberger and von Gersdorff, 2000; Futai et al., 2001; Joshi et al., 2004). Given the presently provided evidence that the C_2 component probably represents a summed spiking activity of MNTB principal cells, a frequency-dependent decrease in C_2 -amplitude for stimulation rates >200 Hz might be indicative of changes in the kinetics of neurotransmitter release, i.e. from fast synchronous transmitter release through rapidly releasing vesicles to slow asynchronous release mediated by the slowly releasing vesicles (Zucker and Regehr, 2002; Sakaba, 2006). This is further corroborated by the finding of a gradual reduction of C_2 amplitude accompanied by a substantial increase in transmission delay (TD) (Fig. 3D). Thus, the depression of fast synchronous release at high input rates probably leads to a substantial desynchronization of postsynaptically evoked spikes which is measured as a decrease in C_2 amplitude. The average transmission delay for the single response was 1.33 ± 0.03 ms. This is a good match with results from paired pre- and postsynaptic patch-clamp recordings in P14–17 mouse (1.34 ms at RT; Fedchyshyn and Wang, 2007). Prolongation of transmission delay and desynchronization of postsynaptic events (increase of C_2 half-width time) presented here possibly relies on depletion of the readily releasable pool of synaptic vesicles. High-frequency stimulation was shown to induce recruitment of additional vesicles from the periphery of the readily releasable pool to the presynaptic Ca^{2+} channel clusters which might account for the increased latency and variations of release events (Wang and Kaczmarek, 1998; Sakaba and Neher, 2001a; Schneggenburger et al., 2002; Sakaba, 2006; Wadel et al., 2007). It is also possible that postsynaptic failures (Guinan and Li, 1990; Kopp-Scheinflug et al., 2003a,b; Hermann et al., 2007), inactivation of presynaptic P-type Ca^{2+} channels upon repetitive stimulation (Forsythe et al., 1998), and postsynaptic AMPA receptor desensitization (Zhang and Trussell, 1994; Wong et al., 2003) contribute to the reduction in amplitude of the C_2 .

4.3. Inhibition in the MNTB revisited by MEA recordings

Several studies *in vitro* and *in vivo* have postulated that MNTB principal cells receive acoustically evoked inhibitory inputs which are able to offset or even impair the postsynaptic spike generation (Guinan and Li, 1990; Banks and Smith, 1992; Wu and Kelly, 1995; Kopp-Scheinflug et al., 2003a; Awatramani et al., 2004, 2005). In mammalian auditory brainstem nuclei, GABAergic and glycinergic neurotransmission shift from depolarizing to hyperpolarizing before the onset of hearing due to an increased activity of the K^+ - Cl^- extruding transporter KCC2 (Balakrishnan et al., 2003; Lohrke et al., 2005; Milenkovic et al., 2007). In line with these findings, GABA and glycine will decrease the input resistance in mature MNTB neurons, possibly lowering the EPSPs to subthreshold levels which then causes a loss of action potential firing (Wu and Kelly, 1995). Here we confirm the inhibitory roles of GABA and glycine in the MNTB, and

we show the developmental down regulation of GABA-mediated effects, along with an enhancement of glycinergic inhibition. A developmental shift from GABA_A-dominated to glycine-dominated transmission has been previously observed in the medial limb of gerbil LSO and in the rat MSO (Kotak et al., 1998; Smith et al., 2000; Nabekura et al., 2004). In the rat MNTB, Awatramani et al. (2005) reported strengthening of glycinergic transmission and increased sensitivity to glycine with maturity, while GABAergic transmission remained relatively constant. From our experiments it is not clear whether the weaker inhibitory effect of GABA perfusion in older animals possibly relies on changes in number, sensitivity, or redistribution of postsynaptic GABA_A receptors. Application of glycine in P20–28 slices reduces the amplitude of the postsynaptic activity, while it increases the amplitude of the presynaptic component. In contrast to its parent cell bodies (globular bushy cell) or its postsynaptic neuron, the calyx of Held has been shown to retain the depolarizing Cl^- gradient across the membrane even after onset of hearing (Price and Trussell, 2006). The increase in C_1 amplitude under glycine is consistent with the activation of presynaptic glycine receptors which causes a depolarization at the calyx and enhances glutamate release (Turecek and Trussell, 2001). Given the reciprocal expression of GABA_A and glycine receptors in developing calyces, with GABA_A-mediated conductance being completely down-regulated by onset of hearing (Turecek and Trussell, 2001, 2002), it is not surprising that in our slice preparations external GABA exhibited only a postsynaptic (C_2) effect on evoked FP.

4.4. Possible extension of MEA applications for auditory brainstem studies

Aside from anatomically discrete inhibitory MNTB-LSO and MNTB-MSO projections (Zook and DiCaprio, 1988; Sanes and Siverls, 1991; Kuwabara and Zook, 1992; Sommer et al., 1993), the anatomical organization of inhibitory circuits contributing to signal processing in the superior olivary complex (SOC) is largely unknown. Possible sources of inhibitory inputs to the MNTB still have to be identified. Investigation of such inhibitory influences by *in vitro* techniques is largely hampered by both anatomical and technical shortcomings. The first relates to the fact that within the SOC functionally different nuclei are located close to each other and the second to the fact that patch clamp recordings are mostly performed at very early postnatal ages and document data from single cells only. Here we demonstrate that *in vitro* recordings by means of MEAs, which enable convenient stimulation of afferent fibers and recording from populations of cells in the subadult MNTB, might be well suited to study circuitries in the auditory brainstem, and could help to identify putative sources of inhibitory projections to the MNTB.

MEA recordings have some advantages over conventional recordings of extracellular field potentials. One of the most straightforward benefits of MEA recordings is the increased throughput owing to the ability to perform long-term stable recordings from multiple sites within one MNTB, and simultaneously from the homonymous nuclei on both sides of the brainstem. This is specifically advantageous in experiments that explore the effects of an additional electrical stimulation (aiming at inhibitory inputs) on field potentials of the MNTB principal cells because the contralateral MNTB can be used as a within-slice control for validation of the experimental results. Furthermore, the simultaneous recording of voltage signals by equally spaced electrodes in the region of the MNTB can be used to acquire the spatiotemporal progression of neuronal activity within this nucleus (Fig. 1B). Utilization of MEA chips with smaller electrode spacing would allow a fine-grained mapping of the dynamics of responses within the MNTB, which could be of interest in studies focussing on specific nuclear

gradients, e.g. tonotopy or graded expression of defined neuronal receptors.

One disadvantage of local field potential recordings is the possible difficulty in interpreting changes in signal components following pharmacological manipulations, in particular when the signals stem from larger populations of neurons which do not show a defined morphological organization. The specific neuronal arrangement has to be considered because the spatial relation of the neurons to the recording electrodes determines the “sources” and “sinks” of the acquired electrical activity, thus influencing the activity profile (Richardson et al., 1987; Gholmieh et al., 2006). Given the aligned organisation of the MNTB principal cells which themselves are lined up in spaces between horizontal fiber bundles (Kuwabara et al., 1991; Kulesza et al., 2002; Rodriguez-Contreras et al., 2006), our study provides a detailed description of the MEA recordings from coronal MNTB slices, and these signals can be directly related to respective extracellular single unit recordings.

Acknowledgments

This work was supported by the Grant MI 954/1-1 and Graduiertenkolleg “InterNeuro”, GRK 1097, both from the Deutsche Forschungsgemeinschaft. Randy Kurz for providing hardware components for measurements. We want to thank Ian Forsythe for critical comments on an earlier version of the manuscript. Additionally, we thank the two anonymous reviewers whose suggestions improved this manuscript.

References

- Awatramani GB, Turecek R, Trussell LO. Inhibitory control at a synaptic relay. *J Neurosci* 2004;24:2643–7.
- Awatramani GB, Turecek R, Trussell LO. Staggered development of GABAergic and glycinergic transmission in the MNTB. *J Neurophysiol* 2005;93:819–28.
- Balakrishnan V, Becker M, Lohrke S, Nothwang HG, Guresir E, Friauf E. Expression and function of chloride transporters during development of inhibitory neurotransmission in the auditory brainstem. *J Neurosci* 2003;23:4134–45.
- Banks MI, Smith PH. Intracellular recordings from neurobiotin-labeled cells in brain slices of the rat medial nucleus of the trapezoid body. *J Neurosci* 1992;12:2819–37.
- Barrett EF, Barrett JN. Intracellular recording from vertebrate myelinated axons: mechanism of the depolarizing afterpotential. *J Physiol* 1982;323:117–44.
- Borst JG, Helmchen F, Sakmann B. Pre- and postsynaptic whole-cell recordings in the medial nucleus of the trapezoid body of the rat. *J Physiol* 1995;489:825–40.
- Casey MA, Feldman ML. Aging in the rat medial nucleus of the trapezoid body. I. Light microscopy. *Neurobiol Aging* 1982;3:187–95.
- Dodson PD, Billups B, Rusznak Z, Szucs G, Barker MC, Forsythe ID. Presynaptic rat Kv1.2 channels suppress synaptic terminal hyperexcitability following action potential invasion. *J Physiol* 2003;550:27–33.
- Egert U, Heck D, Aertsen A. Two-dimensional monitoring of spiking networks in acute brain slices. *Exp Brain Res* 2002a;142:268–74.
- Egert U, Knott T, Schwarz C, Nawrot M, Brandt A, Rotter S, et al. MEA-Tools: an open source toolbox for the analysis of multi-electrode data with MATLAB. *J Neurosci Methods* 2002b;117:33–42.
- Fedchyshyn MJ, Wang LY. Activity-dependent changes in temporal components of neurotransmission at the juvenile mouse calyx of Held synapse. *J Physiol* 2007;581:581–602.
- Forsythe ID. Direct patch recording from identified presynaptic terminals mediating glutamatergic EPSCs in the rat CNS, in vitro. *J Physiol* 1994;479(Pt 3):381–7.
- Forsythe ID, Barnes-Davies M. The binaural auditory pathway: excitatory amino acid receptors mediate dual timecourse excitatory postsynaptic currents in the rat medial nucleus of the trapezoid body. *Proc R Soc Lond B Biol Sci* 1993a;251:151–7.
- Forsythe ID, Barnes-Davies M. The binaural auditory pathway: membrane currents limiting multiple action potential generation in the rat medial nucleus of the trapezoid body. *Proc R Soc Lond B Biol Sci* 1993b;251:143–50.
- Forsythe ID, Tsujimoto T, Barnes-Davies M, Cuttle MF, Takahashi T. Inactivation of presynaptic calcium current contributes to synaptic depression at a fast central synapse. *Neuron* 1998;20:797–807.
- Friauf E, Ostwald J. Divergent projections of physiologically characterized rat ventral cochlear nucleus neurons as shown by intra-axonal injection of horseradish peroxidase. *Exp Brain Res* 1988;73:263–84.
- Futai K, Okada M, Matsuyama K, Takahashi T. High-fidelity transmission acquired via a developmental decrease in NMDA receptor expression at an auditory synapse. *J Neurosci* 2001;21:3342–9.
- Geisler CD, Deng L, Greenberg SR. Thresholds for primary auditory fibers using statistically defined criteria. *J Acoust Soc Am* 1985;77:1102–9.
- Gholmieh G, Soussou W, Han M, Ahuja A, Hsiao MC, Song D, et al. Custom-designed high-density conformal planar multielectrode arrays for brain slice electrophysiology. *J Neurosci Methods* 2006;152:116–29.
- Green JS, Sanes DH. Early appearance of inhibitory input to the MNTB supports binaural processing during development. *J Neurophysiol* 2005;94:3826–35.
- Guinan Jr JJ, Li RY. Signal processing in brainstem auditory neurons which receive giant endings (calyces of Held) in the medial nucleus of the trapezoid body of the cat. *Hear Res* 1990;49:321–34.
- Harrison JM, Irving R. Ascending connections of the anterior ventral cochlear nucleus in the rat. *J Comp Neurol* 1966;126:51–63.
- Hermann J, Pecka M, von Gersdorff H, Grothe B, Klug A. Synaptic transmission at the calyx of Held under in vivo like activity levels. *J Neurophysiol* 2007;98:807–20.
- Isaacson JS. GABAB receptor-mediated modulation of presynaptic currents and excitatory transmission at a fast central synapse. *J Neurophysiol* 1998;80:1571–6.
- Johnston D, Wu SM. Extracellular field recordings. In: Foundations of cellular neurophysiology. Cambridge, MA, USA: MIT Press; 1995.
- Joshi I, Wang LY. Developmental profiles of glutamate receptors and synaptic transmission at a single synapse in the mouse auditory brainstem. *J Physiol* 2002;540:861–73.
- Joshi I, Shokrala S, Titis P, Wang LY. The role of AMPA receptor gating in the development of high-fidelity neurotransmission at the calyx of Held synapse. *J Neurosci* 2004;24:183–96.
- Kajikawa Y, Saitoh N, Takahashi T. GTP-binding protein beta gamma subunits mediate presynaptic calcium current inhibition by GABA(B) receptor. *Proc Natl Acad Sci USA* 2001;98:8054–8.
- Kopanitsa MV, Afinowi NO, Grant SG. Recording long-term potentiation of synaptic transmission by three-dimensional multi-electrode arrays. *BMC Neurosci* 2006;7:61.
- Kopp-Scheinpflug C, Dehmel S, Dorrscheidt GJ, Rubsamen R. Interaction of excitation and inhibition in anteroventral cochlear nucleus neurons that receive large endbulb synaptic endings. *J Neurosci* 2002;22:11004–18.
- Kopp-Scheinpflug C, Lippe WR, Dorrscheidt GJ, Rubsamen R. The medial nucleus of the trapezoid body in the gerbil is more than a relay: comparison of pre- and postsynaptic activity. *J Assoc Res Otolaryngol* 2003a;4:1–23.
- Kopp-Scheinpflug C, Fuchs K, Lippe WR, Tempel BL, Rubsamen R. Decreased temporal precision of auditory signaling in Kcna1-null mice: an electrophysiological study in vivo. *J Neurosci* 2003b;23:9199–207.
- Kotak VC, Korada S, Schwartz IR, Sanes DH. A developmental shift from GABAergic to glycinergic transmission in the central auditory system. *J Neurosci* 1998;18:4646–55.
- Kulesza RJ, Vinuela A, Saldana E, Berrebi AS. Unbiased stereological estimates of neuron number in subcortical auditory nuclei of the rat. *Hear Res* 2002;168:12–24.
- Kuwabara N, Zook JM. Projections to the medial superior olive from the medial and lateral nuclei of the trapezoid body in rodents and bats. *J Comp Neurol* 1992;324:522–38.
- Kuwabara N, DiCaprio RA, Zook JM. Afferents to the medial nucleus of the trapezoid body and their collateral projections. *J Comp Neurol* 1991;314:684–706.
- Leao RM, Kushmerick C, Pinaud R, Renden R, Li GL, Taschenberger H, et al. Presynaptic Na⁺ channels: locus, development, and recovery from inactivation at a high-fidelity synapse. *J Neurosci* 2005;25:3724–38.
- Liberman MC. Auditory-nerve response from cats raised in a low-noise chamber. *J Acoust Soc Am* 1978;63:442–55.
- Lin Y, Chen C, Chen L, Zeng S, Luo Q. The analysis of electrode-recording-horizon in multi-electrode array (MEA). *Conf Proc IEEE Eng Med Biol Soc* 2005;7:7345–8.
- Lohrke S, Srinivasan G, Oberhofer M, Doncheva E, Friauf E. Shift from depolarizing to hyperpolarizing glycine action occurs at different perinatal ages in superior olivary complex nuclei. *Eur J Neurosci* 2005;22:2708–22.
- Mapelli J, D'Angelo E. The spatial organization of long-term synaptic plasticity at the input stage of cerebellum. *J Neurosci* 2007;27:1285–96.
- Milenkovic I, Witte M, Turecek R, Heinrich M, Reinert T, Rubsamen R. Development of chloride-mediated inhibition in neurons of the anteroventral cochlear nucleus of gerbil (*Meriones unguiculatus*). *J Neurophysiol* 2007;98:1634–44.
- Morest DK. The collateral system of the medial nucleus of the trapezoid body of the cat, its neuronal architecture and relation to the olivo-cochlear bundle. *Brain Res* 1968;9:288–311.
- Nabekura J, Katsurabayashi S, Kakazu Y, Shibata S, Matsubara A, Jinno S, et al. Developmental switch from GABA to glycine release in single central synaptic terminals. *Nat Neurosci* 2004;7:17–23.
- Novak JL, Wheeler BC. Multisite hippocampal slice recording and stimulation using a 32 element microelectrode array. *J Neurosci Methods* 1988;23:149–59.
- Oertel D. The role of timing in the brain stem auditory nuclei of vertebrates. *Annu Rev Physiol* 1999;61:497–519.
- Oka H, Shimono K, Ogawa R, Sugihara H, Taketani M. A new planar multielectrode array for extracellular recording: application to hippocampal acute slice. *J Neurosci Methods* 1999;93:61–7.
- Price GD, Trussell LO. Estimate of the chloride concentration in a central glutamatergic terminal: a gramicidin perforated-patch study on the calyx of Held. *J Neurosci* 2006;26:11432–6.
- Richardson TL, Turner RW, Miller JJ. Action-potential discharge in hippocampal CA1 pyramidal neurons: current source density analysis. *J Neurophysiol* 1987;58:981–96.

- Rodriguez-Contreras A, de Lange RP, Lucassen PJ, Borst JG. Branching of calyceal afferents during postnatal development in the rat auditory brainstem. *J Comp Neurol* 2006;496:214–28.
- Sakaba T. Roles of the fast-releasing and the slowly releasing vesicles in synaptic transmission at the calyx of held. *J Neurosci* 2006;26:5863–71.
- Sakaba T, Neher E. Calmodulin mediates rapid recruitment of fast-releasing synaptic vesicles at a calyx-type synapse. *Neuron* 2001a;32:1119–31.
- Sakaba T, Neher E. Quantitative relationship between transmitter release and calcium current at the calyx of held synapse. *J Neurosci* 2001b;21:462–76.
- Sanes DH, Siverls V. Development and specificity of inhibitory terminal arborizations in the central nervous system. *J Neurobiol* 1991;22:837–54.
- Schneggenburger R, Sakaba T, Neher E. Vesicle pools and short-term synaptic depression: lessons from a large synapse. *Trends Neurosci* 2002;25:206–12.
- Smith PH, Joris PX, Carney LH, Yin TC. Projections of physiologically characterized globular bushy cell axons from the cochlear nucleus of the cat. *J Comp Neurol* 1991;304:387–407.
- Smith AJ, Owens S, Forsythe ID. Characterisation of inhibitory and excitatory postsynaptic currents of the rat medial superior olive. *J Physiol* 2000;529(Pt 3):681–98.
- Sommer I, Lingenhohl K, Friauf E. Principal cells of the rat medial nucleus of the trapezoid body: an intracellular in vivo study of their physiology and morphology. *Exp Brain Res* 1993;95:223–39.
- Spiro GA, Brownell WE, Zidanic M. Recordings from cat trapezoid body and HRP labeling of globular bushy cell axons. *J Neurophysiol* 1990;63:1169–90.
- Takago H, Nakamura Y, Takahashi T. G protein-dependent presynaptic inhibition mediated by AMPA receptors at the calyx of Held. *Proc Natl Acad Sci USA* 2005;102:7368–73.
- Taschenberger H, von Gersdorff H. Fine-tuning an auditory synapse for speed and fidelity: developmental changes in presynaptic waveform, EPSC kinetics, and synaptic plasticity. *J Neurosci* 2000;20:9162–73.
- Trussell LO. Synaptic mechanisms for coding timing in auditory neurons. *Annu Rev Physiol* 1999;61:477–96.
- Turecek R, Trussell LO. Presynaptic glycine receptors enhance transmitter release at a mammalian central synapse. *Nature* 2001;411:587–90.
- Turecek R, Trussell LO. Reciprocal developmental regulation of presynaptic ionotropic receptors. *Proc Natl Acad Sci USA* 2002;99:13884–9.
- Wadel K, Neher E, Sakaba T. The coupling between synaptic vesicles and Ca(2+) channels determines fast neurotransmitter release. *Neuron* 2007;53:563–75.
- Wang LY, Kaczmarek LK. High-frequency firing helps replenish the readily releasable pool of synaptic vesicles. *Nature* 1998;394:384–8.
- Winter IM, Palmer AR. Responses of single units in the anteroventral cochlear nucleus of the guinea pig. *Hear Res* 1990;44:161–78.
- Wirth C, Luscher HR. Spatiotemporal evolution of excitation and inhibition in the rat barrel cortex investigated with multielectrode arrays. *J Neurophysiol* 2004;91:1635–47.
- Wong AY, Graham BP, Billups B, Forsythe ID. Distinguishing between presynaptic and postsynaptic mechanisms of short-term depression during action potential trains. *J Neurosci* 2003;23:4868–77.
- Wu SH, Kelly JB. Response of neurons in the lateral superior olive and medial nucleus of the trapezoid body to repetitive stimulation: intracellular and extracellular recordings from mouse brain slice. *Hear Res* 1993;68:189–201.
- Wu SH, Kelly JB. Inhibition in the superior olivary complex: pharmacological evidence from mouse brain slice. *J Neurophysiol* 1995;73:256–69.
- Zhang S, Trussell LO. Voltage clamp analysis of excitatory synaptic transmission in the avian nucleus magnocellularis. *J Physiol* 1994;480:123–36.
- Zook JM, DiCaprio RA. Intracellular labeling of afferents to the lateral superior olive in the bat, *Eptesicus fuscus*. *Hear Res* 1988;34:141–7.
- Zucker RS, Regehr WG. Short-term synaptic plasticity. *Annu Rev Physiol* 2002;64:355–405.